J Therm Anal Calorim (2010) 100:529–535
DOI 10.1007/s10973-009-0590-6

Low temperature sintering study of nanosized Mn–Zn ferrites synthesized by sol–gel auto combustion process

H. Waqas · A. H. Qureshi

Received: 3 April 2009 / Accepted: 28 October 2009 / Published online: 15 December 2009

Abstract The objective of present research was to sinter nanosized Mn–Zn ferrites (MZF) at low temperature (≤1,000 °C) by avoiding the formation of nonmagnetic phase (hematite). For this purpose, MZF powder was synthesized by sol–gel auto combustion process at 220 °C and further calcined at 450 °C. In calcined powder, single phase (spinel) was confirmed by X-ray diffraction analysis. Pellets were pressed, having 43% of the theoretical density and showing 47 emu gm^{-1} saturation magnetization (M_s). Various combinations of heating rate, dwelling time and gaseous environment were employed to meet optimum sintering conditions at low temperature (≤1,000 °C). It was observed that sintering under air or N_2 alone had failed to prevent the formation of nonmagnetic (hematite) phase. However, hematite phase can be suppressed by retaining the green compacts at 1,000 °C for 180 min in air then further kept for 120 min in nitrogen. Under these conditions, spinel phase (comprising of nano crystallites), 90% of theoretical density and 102 emu gm^{-1} of saturation magnetization has been achieved.

Keywords Sol–gel auto combustion · Soft ferrite · Oxidation · Reduction · Nano-crystallites · Sintering · X-ray diffraction · SEM · VSM

H. Waqas (✉)
Department of Chemical and Materials Engineering, PIEAS, Nilore, Islamabad, Pakistan
e-mail: hw_pk@yahoo.com

A. H. Qureshi
Materials Division, Directorate of Technology, PINSTECH, Nilore, Islamabad, Pakistan

Introduction

On the basis of crystallographic structure, Mn–Zn ferrites (MZF) come under the category of spinels. In general, spinels are represented by AB_2O_4, where '*A*' may be any divalent cation such as Mn^{2+}, Zn^{2+}, Ni^{2+}, Fe^{2+} etc. and '*B*' denoted trivalent cation such as Fe^{3+}, Mn^{3+} etc. [1]. These magnetically soft materials are well known for their electromagnetic applications and mostly used as core component of electronic transformers, high frequency data transfer devices, charge particle deflection yoke rings etc. [2]. MZF have also proven their importance for spintronic applications [3]. Their transport properties (electrical and magnetic) can be altered either by choosing different synthesis routes [4–7] or by addition/substitution of oxides of third group/rarer metals [1, 8]. The particle size of synthesized powder depends upon processing route while transport properties can be tailored by varying cationic distribution in spinel lattice [9].

Although selective synthesis route and addition/substitution of specific cations are important parameters but the role of sintering in the processing of MZF has its own worth. During the sintering of MZF, formation of nonmagnetic (hematite) phase and the loss of zinc [10, 11] are very common.

The composition ($Mn_{0.57}$ $Zn_{0.35}$ $Fe_{2.08}O_4$) under investigation also contained 0.35 mole fraction of zinc, therefore, the loss of zinc during sintering could not be ignored. Both of these problems act as poison to drop the magnetic properties. These specially decrease the saturation magnetization of MZF by disturbing the cationic (Fe^{+3}) distribution in spinel lattice [12]. Different researchers have [13, 14] tried to overcome these issues by sintering MZF (synthesized by mixed oxide method) at high temperature 1,300–1,400 °C under controlled atmospheres. Although

95–98% of theoretical density was obtained but the saturation magnetization (M_s) could not be enhanced more than 80–85 emu gm^{-1}. Similarly for other synthesis routes such as co-precipitation, hydrothermal and sol–gel, more or less the similar properties were obtained by sintering at relatively lower temperature (≤1,200 °C) [15].

The current investigations deal with low temperature (≤1,000 °C) sintering study of nanosized MZF synthesized by sol–gel auto combustion process. The effect of sintering parameters such as gaseous environment, sintering time and heating rate on the growth of magnetic (spinel) phase have been discussed. The possible reaction mechanisms that involves during sintering like reactivity of nano crystallite, oxidation/reduction of magnetic phase and zinc loss in MZF have also been enlightened.

Experimental

Mn–Zn ferrite ($Mn_{0.57}Zn_{0.35}Fe_{2.08}O_4$) was synthesized by sol–gel auto combustion process. The important steps involve during the synthesis process are mentioned in Fig. 1. Complete synthesis detail is available elsewhere [16]. Chemical reaction that helps to produce magnetic phase by sol–gel auto combustion process is given in Eq. 1 [17]:

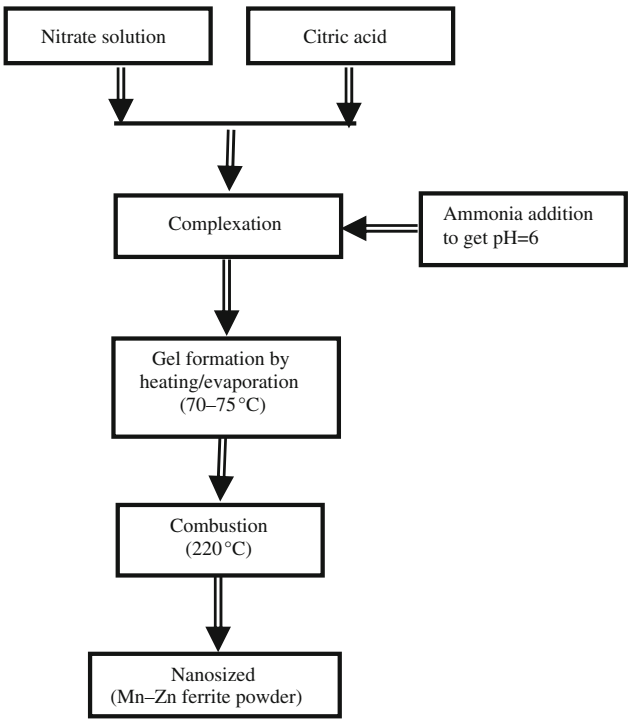

Fig. 1 Flow chart of sol–gel auto combustion process

$$2Fe(NO_3)_3 + xMn(NO_3) + (1-x)Zn(NO_3)_2 + 3C_6O_7H_8 + 8HNO_3 + 9.5O_2 \rightarrow (Mn_xZn_{1-x})Fe_2O_y + 18CO_2 + 8N_2 + 24H_2O. \quad (1)$$

The combustion powder was calcined at 450 °C and pellets were obtained by uniaxial press. These green pellets were designated as A1 to A10 and sintered in carbolite tube furnace (MTF-10/25/130) attached with gas controller (D08-4C) under different environments as given in Table 1. Bruker (D-5005) X-ray diffractometer (XRD) with Cuk_α, having $\lambda = 1.5406$ Å was used to identify magnetic phase. Lakeshore (model-3500) vibrating sample magnetometer (VSM) system was employed to measure saturation magnetization (M_s) of both green and sintered pellets at room temperature. Scanning electron microscope (LEO-40) and energy dispersive X-ray (EDX) analysis were used to obtain micrographs and elemental composition of selected sintered pellets (A3 and A10), respectively.

Results and discussion

Formation of nanosized Mn–Zn ferrite powder

In sol–gel auto combustion process [17, 18], self propagation combustion reaction was completed in the range 200–220 °C and further heated (calcine) at 450 °C for 20 min to remove the unwanted species. The XRD patterns of gel, combustion and calcined powders are shown in Fig. 2. By using the Scherrer's formula [19], particle size of calcined powder (single phase) was calculated as 26 ± 3 nm from the strongest peak (311) in the XRD spectrum (Fig. 2). With some minor difference, d-values of the calcined powder were close to Franklinite phase (JCPD card no.10-0467). This minor difference might be due to the distortion of $ZnFe_2O_4$ lattice by partial diffusion of Mn ions. After pressing the calcined powder in form of pellet, green density was 2.88 gm cm^{-3}, while the saturation magnetization was measured as 47 emu gm^{-1}. These results revealed that single phase (spinel) nanosized ferrite powders can be synthesized at low temperature (220 °C) by sol–gel auto combustion process. This is in contrast to conventional ceramic route [1] in which spinel phase is obtained at high temperature (900–1300 °C) by employing the calcination and sintering processes.

Sintering study

The most common problem during the sintering of sol–gel auto combustion product is to retain spinel phase (developed during combustion) because it partially oxidizes/decomposes into nonmagnetic (hematite) phase according to Eq. 2 [20]:

Table 1 Parameters for sintering nanosized Mn–Zn ferrite pellets

Pellet ID.	Sintering temp./°C	Sintering time/min	Heat rate/°C min^{-1}	Gas supplied
Sintering in air or nitrogen				
A1	950	120	10	Air
A2	950	180	10	Air
A3	1000	300	10	Air
A4	950	120	10	N_2
A5	950	180	10	N_2
A6	950	120	10	N_2-supply from 700 °C
A7	950	180	10	N_2-supply from 700 °C
Sintering with combination of air and nitrogen				
A8	1,000	240 min in air and 60 min in N_2	100	Air/N_2
A9	1,000	210 min in air and 90 min in N_2	100	Air/N_2
A10	1,000	180 min in air and 120 min in N_2	100	Air/N_2

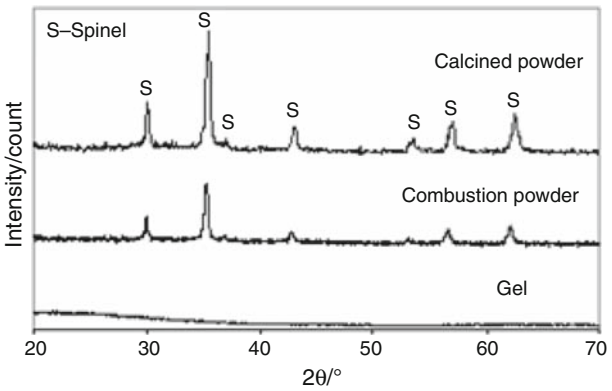

Fig. 2 XRD spectrums of gel, combustion and calcined (450 °C for 20 min) Powders [16]

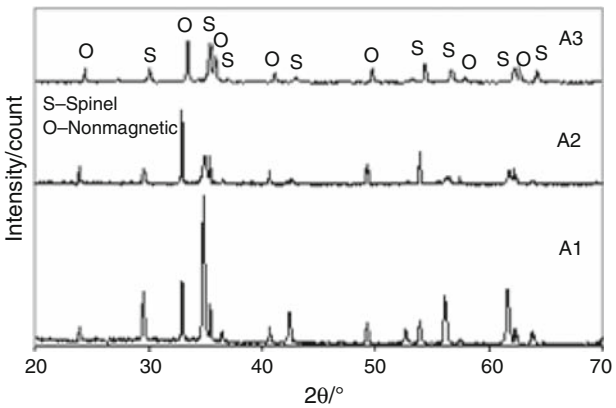

Fig. 3 XRD spectrums of calcined pellets A1, A2 and A3 sintered in air

$$4Fe_3O_4 + O_2 \longleftrightarrow 6Fe_2O_3 \quad \text{(magnetite)} \qquad \text{(hematite)}. \tag{2}$$

The presence of hematite lowers down saturation magnetization of sintered product. In order to overcome this problem different sintering procedures were adopted.

Sintering in air or nitrogen

Green pellets as designated by A1, A2 and A3 (Table 1) were sintered in air by varying time (60–300 min) and temperature (950–1,000 °C). It was observed that the pellets turned black after sintering in air and peaks of hematite phase were detected in XRD pattern as shown in Fig. 3. It might be due to the partial oxidation of ferrite phase in the presence of air according to Eq. 3 [21]:

$$Zn_{1-x}Mn_xFe_2O_4 + X/4\ O_2 \longleftrightarrow (1-X)\ ZnFe_2O_4 + X/2\ MnO_3 + XFe_2O_3 \quad \text{(hematite)}. \tag{3}$$

In further study, pellets A4 and A5 (Table 1) were sintered at 950 °C in nitrogen environment to avoid oxidation of spinel phase. The pellets turned reddish in the presence of nitrogen that was again the indication of ferric oxide (iron III) phase as shown in XRD results (Fig. 4). The creation of nonmagnetic phase was due to the reduction of ferrites in nitrogen atmosphere as described by Neijts [22] in Eq. 4:

$$MnFe_2O_4 \rightarrow MnO_x + Fe_2O_3 \quad \text{(Spinel)} \qquad \text{(hematite)}. \tag{4}$$

These results revealed that the formation of hematite phase in MZF could not be avoided when sintered in air or nitrogen alone at $\leq$1,000 °C.

Sintering with combination of air and nitrogen

Vladimirtseva and Soltyk [23] investigated that maximum oxidation of spinel phase occurred between 600 and 800 °C, therefore, to avoid oxidation, nitrogen was supplied from 700 °C during the sintering (950 °C for 120 min) of pellet A6 (Table 1). The XRD result of A6 shown in Fig. 5 although confirmed the dominancy of

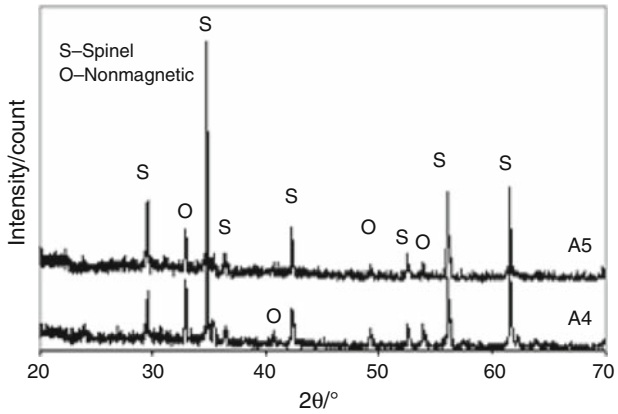

Fig. 4 XRD spectrums of pellets A4 and A5 sintered in nitrogen

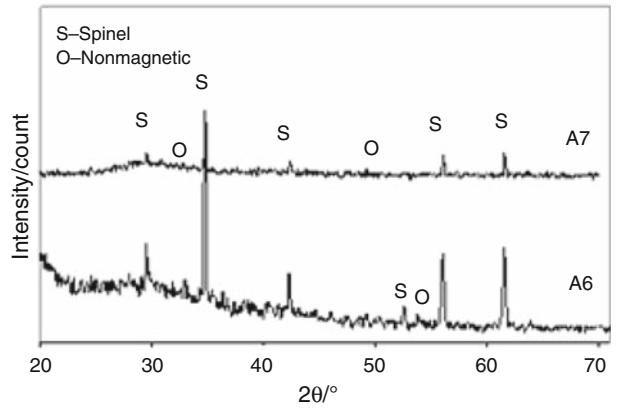

Fig. 5 XRD spectrums of pellets A6 and A7 sintered in nitrogen supplied from 700 °C

spinel phase but still some peaks of hematite are present in it. In another experiment, pellet (A7) was sintered at 1,000 °C with faster heating rate of 100 °C min^{-1} and nitrogen was supplied from 700 °C during heating. It was observed that nonmagnetic phase had been remarkably suppressed (Fig. 5).

The above results indicated that sintering at 1,000 °C under appropriate conditions may help to overcome the problem of spinel phase transformation to nonmagnetic (hematite) phase. Therefore further sintering was conducted at 1,000 °C.

The pellets A8, A9 and A10 (Table 1) were sintered at 1,000 °C in air for 240, 210 and 180 min then in nitrogen for further 60, 90 and 120 min, respectively. It was observed from XRD results (Fig. 6) that as the exposure time of nitrogen was increased the volume fraction of hematite phase decreased and completely vanished by exposing the pellet (A10) in nitrogen for 120 min. Thus, single phase (spinel) structure was obtained in pellet (A10).

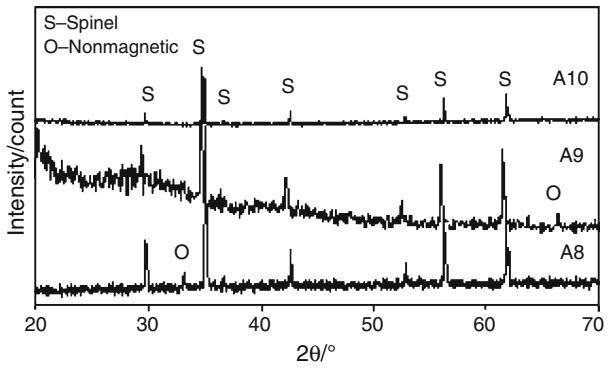

Fig. 6 XRD spectrums of pellets A8, A9 and A10 sintered in air and nitrogen

In sintered pellet A10, shifting of peaks from higher angles side to lower angles was observed in XRD spectrum (Fig. 6). This shifting was due to the complete transformation of $ZnFe_2O_4$ to $MnZnFe_2O_4$. The enough sintering time (240 min in air + 120 min in nitrogen) and temperature (≤1,000 °C) enhanced the diffusion of Mn ions in $ZnFe_2O_4$ lattice that allowed to form MZF as described by Bozadjiev et al. [2]. By matching the *d*-values of A10 with XRD master data, Jacobsite Zincian (JCPD card no. 74-2401) phase was identified. The sintered density of A10 was measured as 4.54 gm cm^{-3}, i.e. 90% of the theoretical density of MZF. Hence, low temperature (≤1,000 °C) sintering of nanosized MZF was achieved by adjusting the dwelling time in both oxidizing (air) and inert (N_2) atmospheres. The optimum sintering cycle is shown in Fig. 7.

In the view of aforementioned discussion, mechanism behind low temperature (≤1,000 °C) sintering of nanosized MZF can be explained on the basis of two phenomenons.

One is the highly reactive nature of nanosized combustion powder that helps to decrease the sintering temperature. As it has been observed [13, 17] that in sol–gel auto combustion process, high temperature is attained for short time and then rapidly cooled down to room

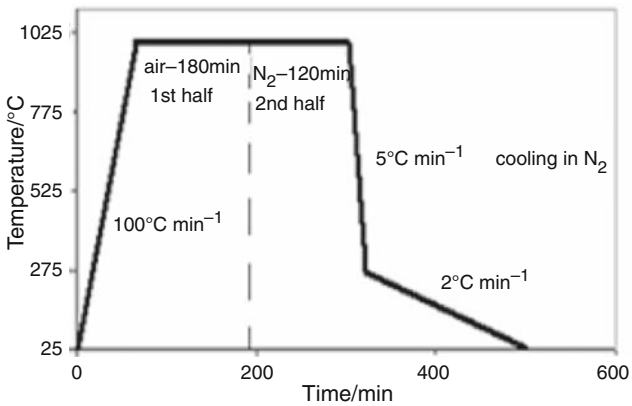

Fig. 7 Optimum sintering cycle

temperature. This phenomenon produces lattice and surface defects within synthesized powder. These high energy restoring points (defects) help to enhance the reactivity of powder particles that resulted to lower down the sintering temperature.

The second assumption based upon the possibility of oxidation/reduction of ferrite powder during different stages of sintering. Present studies showed that in first half of sintering cycle (Fig. 7) air had provided maximum opportunity for the oxidation of spinel phase according to Eq. 3. While inert atmosphere (N_2) in second half of cycle had not only favoured the reduction process by reversing the reaction (Eq. 3) but also helped to improve the sintered density as suggested by Drofenik and coworkers [24]. Hence, it can be attributed that after a suitable time, switching from static air to inert (N_2) atmosphere promotes the sintering of nanosized MZF at 1,000 °C.

Saturation magnetization

Saturation magnetization (M_s) is one of the promising magnetic properties. For each sintered pellets 'M_s' value was determined (Table 2). These values fall in the range of 2–102 emu gm^{-1}. It had been observed that the formation of nonmagnetic phase (hematite) during the sintering process was responsible to drop down the M_s value. In order to verify this assumption the fraction of nonmagnetic phase (hematite) in sintered pellets was calculated from the relevant intensity (I) data of each phase by using the Eq. 5 [25]:

$$\% \text{ Nonmagnetic phase (hematite)} = \left[I_{\text{hematite}} / \left(I_{\text{hematite}} + I_{\text{spinel}}\right)\right] \times 100. \quad (5)$$

The plot of M_s against the fraction of non magnetic phase (hematite) is shown in Fig. 8. From this figure, it is quite clear that as the fraction of hematite decreases the value of saturation magnetization increases. The pellet (A10) that was free from hematite phase attained maximum M_s value 102 emu gm^{-1}. On the basis of this investigation, it can be inferred that the saturation magnetization of a specific composition is a function of sintering conditions. The favorable sintering conditions assist to improve the saturation magnetization to manifold.

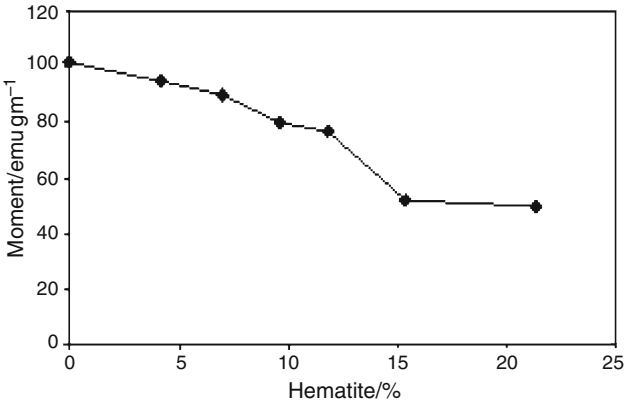

Fig. 8 Saturation magnetization (M_s) as a function of nonmagnetic phase (hematite)

Table 2 Saturation magnetization of Mn–Zn ferrite against volume fraction of magnetic phase

Pellet ID.	Magnetic phase (Spinel)	Sat. Mag. (M_s)/emu gm^{-1}
A1	26	6
A2	24	4
A3	20	2
A4	78.64	50
A5	84.65	52
A6	88.18	77
A7	90.38	80
A8	93	90
A9	95.8	95
A10	100	102

SEM and EDX analyses

In order to quantify the zinc content in sintered products, EDX analysis was employed on A3 and A10 having minimum (2 emu gm^{-1}) and maximum (102 emu gm^{-1}) saturation magnetizations, respectively. SEM micrographs of these pellets are shown in Fig. 9a, b and their respective EDX analyses are given in Table 3. From EDX results it can be observed that the pellet (A3) sintered at 1,000 °C for 300 min in air has lost 32.7% of the total zinc mass. While the SEM micrograph (Fig. 9a) of A3 (etched with HNO_3/HF/DMW, 3:1:16) is showing platelets of hematite phase [26]. Thus, both of these problems (loss of zinc and the partial oxidation of spinel phase) were responsible for the extremely low saturation magnetization (2 emu gm^{-1}). While for pellet (A10) that was sintered under optimum conditions (Fig. 7) attained highest saturation magnetization (102 emu gm^{-1}). It was due to the minor zinc loss (0.80%) and absence of iron oxide (Fe_2O_3) platelets (Fig. 9b). In order to further investigate the effect of sintering, another SEM micrograph of A10 was obtained at higher magnification (60,000×) as shown in Fig. 10. It can be observed that the spherical particles of approximately 32-nm size are acting as building blocks to construct larger grains (~500 nm). Hence, this well organized/homogenized internal structure with minimum zinc loss plays a crucial role to attain higher saturation magnetization.

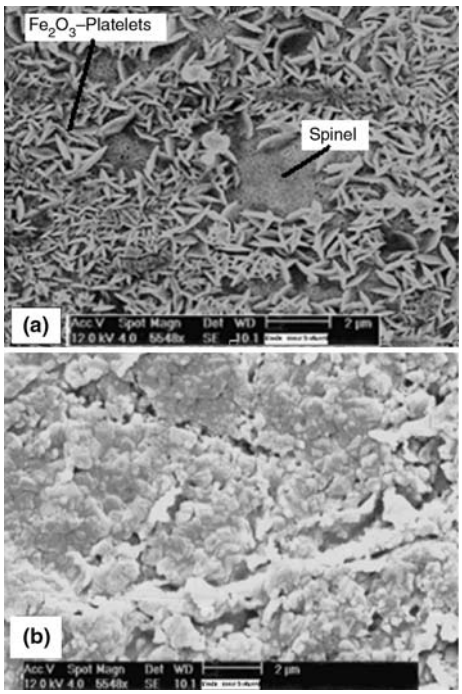

Fig. 9 **a–b** SEM micrographs of sintered pellets A3 and A10

Table 3 EDX analyses of sintered pellets A3 and A10

Elements	Elemental mass% in Pellet (A3)	Elemental mass% in Pellet (A10)
Fe	72.90	70.00
Mn	17.02	16.61
Zn	9.08	13.38

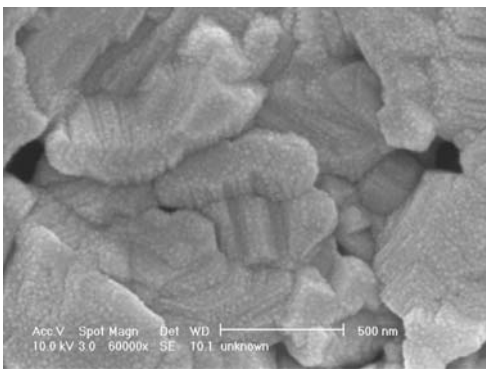

Fig. 10 SEM micrograph of A10 depicting nano particles inside larger grains

Conclusions

Nanosized MZF powder synthesized by sol–gel auto combustion can be sintered at low temperature (≤1,000 °C) in contrast to conventional ceramic method that required high sintering temperature (1,200–1,300 °C). The selection of appropriate sintering parameters (time, temperature and gaseous environment) resulted in sintered products bearing good density, single phase (spinel) and minor zinc loss that help to popup the saturation magnetization of sintered Mn–Zn ferrite.

Acknowledgements Many thanks to Pakistan Higher Education Commission (HEC) for its financial support. Author would also like to acknowledge National University of Singapore (NUS) for providing the opportunity of research at the Department of Materials Science and Engineering.

References

1. Qureshi AH. The influence of hafnia and impurities (CaO/SiO_2) on the microstructure and magnetic properties of Mn–Zn ferrites. J Cryst Growth. 2006;286:365–70.
2. Bozadjiev L, Dimova T, Doynov M. Solid solutions in the system jacobcite $MnFe_2O_4$–franklinite $ZnFe_2O_4$. Geosciences 2006;131–134.
3. Tomar MS, Singh SP, Perales-Perez O, Guzman RP, Calderon E, Rinaldi-Ramos C. Synthesis and magnetic behavior of nanostructured ferrites for spintronics. Microelectron J. 2005;36:475–9.
4. Bueno AR, Gregori ML, Nóbrega MCS. Effect of Mn substitution on the microstructure and magnetic properties of $Ni_{0.50-x}Zn_{0.50-x}Mn_{2x}Fe_2O_4$ ferrite prepared by the citrate–nitrate precursor method. Mater Chem Phys. 2007;105:229–33.
5. Jeyadevan B, Tohiji K, Nakatsuka K, Narayanasamy A. Irregular distribution of metal ions in ferrites prepared by co-precipitation technique structure analysis of Mn–Zn ferrite using extended X-ray absorption fine structure. J Magn Magn Mater. 2000;217:99–105.
6. Hou J, Qu Y, Ma W, Sun Q. Effect of CuO–Bi_2O_3 on low temperature sintered MnZn-ferrite by sol–gel auto-combustion method. Sol-Gel Sci Technol. 2007;44:15–20.
7. Wang H, Kung S. Crystallization of nanosized Ni–Zn ferrite powders prepared by hydrothermal method. J Magn Magn Mater. 2004;270:230–6.
8. Ahmed MA, Okasha N, El-Sayed MM. Enhancement of the physical properties of rare-earth-substituted Mn–Zn ferrites prepared by flash method. Ceram Int. 2007;33:49–58.
9. Tangsali RB, Keluskar SH, Niak GK, Budkuley JS. Effect of sintering conditions on resistivity of nanoparticle Mn–Zn ferrite prepared by nitrilotriacetate precursor method. J Mater Sci. 2007;42:878–82.
10. Inaba H, Matsui T. Vaporization and diffusion of manganese–zinc ferrite. J Sol Stat Chem. 1996;121:143–8.
11. Hofmann MH, Campbell SJ, Ehrhardt H, Feyerherm R. The magnetic behaviour of nanostructured zinc ferrite. J Mater Sci. 2004;39:5057–65.
12. Rath C, Anand S, Das RP, Sahu KK, Kulkarni SD, Date SK, et al. Dependence on cation distribution of particle size, lattice parameter, and magnetic properties in nanosize Mn–Zn ferrite. J Appl Phys. 2002;91:2211–5.
13. Agraflotis CC, Zaspalis VT. Self-propagating high-temperature synthesis of MnZn-ferrites for inductor applications. J Magn Magn Mater. 2004;283:364–74.
14. Rosales MI, Plata AM, Nicho ME, Brito A, Ponce MA. Effect of sintering conditions on microstructure and magnetic properties of Mn–Zn ferrites. J Mater Sci. 1995;30:4446–50.
15. Limin D, Zhidong H, Yaoming Z, Ze W, Xianyou Z. Preparation and sinterability of Mn–Zn ferrite powders by sol-gel method. J Rare Earths. 2006;24:54–6.

16. Waqas H, Qureshi AH. Influence of pH on nanosized Mn–Zn ferrite synthesized by sol-gel auto combustion process. J Therm Anal Calorim 2009;98:355–60.
17. Lorentzou S, Agraflotis CC, Konstandopoulos AG. Aerosol spray pyrolysis synthesis of water-splitting ferrites for solar hydrogen production. Granul Matter. 2008;10:113–22.
18. Azadmanjiri J. Preparation of Mn–Zn ferrite nano particles from chemical sol–gel combustion method and the magnetic properties after sintering. J Non-Cryst Sol. 2007;353:4170–3.
19. Shabbir G, Qureshi AH, Saeed K. Nano-crystalline $LaFeO_3$ powders synthesized by the citrate-gel method. Mater Lett. 2006;60:3706–9.
20. Broussaud M, Abouaf M, Perriat P, Rolland JL. Advances in ferrites. ICF5. 1989;5:75–81.
21. Rozman M, Drofenik M. Microwave-hydrothermal synthesis of nanophase ferrites. J Am Ceram Soc. 1995;9:2449–55.
22. Neijts RC, Advances in ferrites. Internal Philips Report, 1989;1179–1184.
23. Vladimirtseva LA, Soltyk VE. Relationship between the phase composition and technological characterization of Mn–Zn ferrite powders. Porosh Metall. 1972;7:45–50.
24. Rozman M, Drofenik M. Sintering of nanosized Mn–Zn ferrite powders. J Am Ceram Soc. 1998;81:1757–64.
25. Arhad M, Qureshi AH. Time and temperature base study for the production of high T_c phase by sol–gel technique in Pb-BSCCO system. J Therm Anal Calorim. 2006;83:415–9.
26. Huijbregts WMM, Microscopy at the boiler corrosion research. Electrical 1971;49:254–259 (translated from Dutch).